Direct probing of temperature-independent bulk half-metallicity in Co_2MnSi by spin-resolved hard x-ray photoemission

Shigenori Ueda,[1,2,3,*] Yoshio Miura,[4,5] Yuichi Fujita,[4,6] and Yuya Sakuraba[4]

[1]*Research Center for Functional Materials, National Institute for Materials Science (NIMS), Tsukuba, Ibaraki 305–0044, Japan*

[2]*Reserach Center for Advanced Measurement and Characterization, NIMS, Tsukuba, Ibaraki 305–0047, Japan*

[3]*Synchrotron X-ray Station at SPring-8, NIMS, Sayo, Hyogo 679–5148, Japan*

[4]*Research Center for Magnetic and Spintronic Materials, NIMS, Tsukuba, Ibaraki 305–0047, Japan*

[5]*Center for Spintronics Research Network, Graduate School of Engineering Science, Osaka University, Toyonaka, Osaka 560–8531, Japan*

[6]*International Center for Young Scientists, NIMS, Tsukuba, Ibaraki 305–0047, Japan*

(Received 8 April 2022; revised 27 May 2022; accepted 8 July 2022; published 1 August 2022)

We have performed the bulk-sensitive spin-resolved hard x-ray photoelectron spectroscopy (HAXPES) to directly clarify the spin-dependent valence band electronic states and spin polarization of $L2_1$-ordered Co_2MnSi as a predicted half-metal. The spin-resolved valence band HAXPES spectra clearly exhibited the difference in the majority and minority spin states in the bulk region of a 30-nm-thick $Co_2MnSi(001)$ thin film buried under a MgO(2 nm) layer at both temperatures of 21 and 300 K. As expected from the half-metallicity in Co_2MnSi, we found that the majority (minority) spin spectrum shows a metallic Fermi edge (a band gap), leading the high spin polarization of ∼90% at around the Fermi level at a temperature of 21 K. The spin-resolved HAXPES experiments revealed that the half-metallicity of Co_2MnSi in the bulk region is independent on the temperature up to 300 K. The experiments also revealed the slight changes in the majority spin spectral shapes and the shift of the valence band maximum of the minority spin states with temperature. By comparing the experimental results with the first-principles calculations at a finite temperature obtained by the disordered local moment method, it is suggested that the slight changes in the majority and minority spin HAXPES spectra of Co_2MnSi with temperature is mainly caused by the temperature-dependent Co 3*d* electronic states. It is also suggested that the conduction band minimum of the minority spin states is located sufficiently above the Fermi level at temperature up to 300 K.

DOI: 10.1103/PhysRevB.106.075101

I. INTRODUCTION

Heusler alloys, which are represented by X_2YZ (X and Y are transition metal elements, and Z is main-group elements), have a great potential for applications such as spintronics [1], thermoelectronics [2], magnetic shape memory alloys [3], and catalysts [4] due to a huge combination of X, Y, and Z elements. Strong reduction in the minority spin density of states (DOS) at around the Fermi level (E_F) for Co_2MnAl and Co_2MnSn was theoretically recognized by Kübler *et al.* [5], so that they concluded that the electrical transport properties in these alloys were dominated by the majority spin electrons. Owing to the peculiar transport properties in these alloys, exploring of half-metals, in which one spin state is metallic and the other spin state is insulating, has been extensively done for Heusler alloys by theoretical calculations, and several Co-based Heusler alloys are predicted as a half-metal [6–9]. Half-metallic Co-based Heusler alloys are promising materials for practical spintronic device applications due to 100% spin polarization (*SP*) at the E_F and high Curie temperature sufficiently above room temperature (*RT*) in these materials [1,6–9]. The direct observation of the *SP* at E_F for the predicted half-metals at low and high temperatures (T) is important to develop the performance of spintronic devices, because the strong reduction of performance at *RT* compared to low T in tunnel and current-perpendicular-to-plane giant magnetoresistance (TMR and CPP-GMR) junctions [1,10–13] is a long-standing issue to be solved. For example, the $Co_2MnSi/MgO/Co_2MnSi$ TMR junction exhibited that the a huge TMR ratio of 683% at 4.2 K reduced to 179% at *RT* [11], and the $Co_2Fe(Al_{0.5}Si_{0.5})/Ag/Co_2Fe(Al_{0.5}Si_{0.5})$ CPP-GMR junction exhibited that a large GMR ratio of 80% at 14 K reduced to 34% at 290 K [13]. However, the methods for detecting the *SP* at E_F of materials are severely limited. The point contact Andreev reflection (PCAR) measurement gives the *SP* at E_F of materials, but the value of *SP* is affected by the contact between the superconducting probe and target materials, and is also affected by the conduction modes (ballistic or diffusive) in materials [14,15]. In addition, the PCAR measurement, in principle, requires a superconducting probe, so that the measurement is limited by the superconducting critical T (T_C) of superconductors and cannot access higher T

*Corresponding author: UEDA.Shigenori@nims.go.jp

above T_C. The sign of the anisotropic and ordinary MR (AMR and OMR) can indicate the possibility of half-metallicity, and can be applicable to the T-dependent measurements [16–19]. However, both the AMR and OMR measurements do not give the quantitative value of SP at E_F of materials.

To directly observe the SP of the valence band for predicted half-metals, spin-resolved photoelectron spectroscopy (PES) is expected to be a powerful tool. Several spin-resolved PES results for Co_2MnSi as a predicted half-metal have been reported up to now [20–24], but the results reflected the surface-sensitive spin-resolved electronic states, which were strongly affected by surface termination and surface resonance, due to the short inelastic mean-free-path (IMFP) of photoelectrons excited by vacuum ultraviolet (VUV) light sources [20,22,23]. In addition, the SP depends on the photon polarization in spin-resolved PES using VUV light sources [20,24], whereas spin-resolved PES for Co_2MnSi using an unpolarized He-I light source exhibited high SP of ∼0.93 (∼93%) at E_F [21]. Jourdan *et al.* claimed that the highly spin-polarized surface resonance on the $Co_2MnSi(001)$ surface extended over the 6 atomic layers (∼0.6 nm) from the top surface and it strongly connected to bulk majority spin band from the theoretical calculations [21]. Angle-resolved photoemission spectroscopy (ARPES) with spin resolution for the excitation photon energy ($h\nu$) of 6.05 eV clearly showed the highly spin-polarized states near E_F [23], and spin-integrated surface-sensitive soft x-ray ARPES ($h\nu = 1.0$ keV) revealed the band dispersion of the surface resonance near the Γ point, which differed from the bulk band dispersion [25]. However, the bulk band dispersion was clearly found in spin-integrated bulk-sensitive ARPES measurements ($h\nu = 3.3$ keV) for $Co_2MnSi(001)$ [23]. Therefore, more bulk-sensitive spin-resolved electronic structure measurements compared to the previously reported spin-resolved PES results [20–24] are required to probe the nature of SP in bulk Co_2MnSi. Since IMFP increases with increasing the kinetic energy of photoelectrons in solids, hard x-ray PES (HAXPES) is a powerful tool for detecting bulk-sensitive electronic states of materials [26–29]. Recent progress of HAXPES enables us to conduct spin-resolved valence band HAXPES experiments [30–32]. In this work, to reveal the half-metallicity and the SP at E_F of Co_2MnSi in the bulk region, we have applied spin-resolved HAXPES to directly probe the bulk-sensitive spin-resolved valence band electronic states at $T = 21$ and 300 K, and the observed results are compared with the T-dependent electronic structures obtained by first-principles calculations.

II. EXPERIMENT

A. Sample preparation and characterization

We used an ultrahigh vacuum (UHV) sputtering system consisting of two connected chambers for DC and RF sputtering with base pressures (P_{base}) of $\sim 8 \times 10^{-7}$ Pa and $\sim 3 \times 10^{-6}$ Pa, respectively, to fabricate an epitaxial $Co_2MnSi(001)$ film. First, we cleaned a MgO(001) single-crystalline substrate with acetone, isopropanol, and deionized water in an ultrasonicator in advance, then annealed at 600 °C for 30 min in the RF sputtering chamber. Next, a 30-nm-thick Co_2MnSi film was deposited on the MgO(001) substrate using a $Co_{42.8}Mn_{29.4}Si_{27.9}$-alloy target in the DC sputtering chamber, followed by post-deposition annealing at 550 °C for 30 min in the RF sputtering chamber. The actual chemical composition of the Co_2MnSi film was confirmed to be $Co_{2.09}Mn_{0.94}Si_{0.97}$ by using x-ray florescence spectroscopy, indicating the formation of a stoichiometric Co_2MnSi layer. On the top of the $Co_2MnSi(001)$ film, a 2-nm-thick MgO capping layer was deposited using a MgO target through RF sputtering. The sputtering rate and pressure for the depositions of the Co_2MnSi film (the MgO capping layer) were set to be ∼0.18 Å/s (∼0.035 Å/s) and ∼0.11 Pa (∼0.20 Pa), respectively. Using a conventional x-ray diffraction (XRD) method with Cu $K\alpha$ radiation, we clearly confirmed a 002 superlattice peak from $B2$ ordering and a 111 superlattice peak from $L2_1$ ordering of the Co_2MnSi film in θ-2θ XRD profiles by setting the scattering vector to the out-of-plane ($\chi = 0°$) and the {111} plane ($\chi = 54.7°$), respectively, suggesting the epitaxial growth of the Co_2MnSi film. Further, we measured the field dependence of magnetization (M-H curve) for the Co_2MnSi film at 20 and 300 K. The coercivity and the remanent to saturation magnetization ratio deduced from the M-H curve at 20 (300) K are ∼8.5 (∼5.8) Oe and 0.98 (0.97), respectively.

B. Spin-resolved HAXPES

Bulk-sensitive spin-resolved HAXPES was conducted at the revolver undulator beamline BL15XU of SPring-8 [33]. The 2-nm-thick MgO capped epitaxial Co_2MnSi thin film with the thickness of 30 nm was used as a sample. The sample was *in situ* magnetized by an applied magnetic field of 0.3 T using a Nd-Fe-B permanent magnet in an UHV analysis chamber of HAXPES with $P_{base} < 2 \times 10^{-7}$ Pa attached to a high-resolution hemispherical electron analyzer (VG Scienta, R4000). We measured the valence band spectrum (I_+) for the remanently magnetized sample with the in-plane magnetization direction nearly parallel to x-rays. We also measured the spectrum (I_-) for the sample with the opposite magnetization direction. The spin direction of the excited photoelectrons was selected by a Mott-type spin-filter using the Au thin film [31]. To obtain the spin-resolved HAXPES spectra, the magnetization reversal of the sample was essentially required in this method, so that we conducted the magnetization reversal several times at each T. The effective Sherman function (S_{eff}) of −0.07 was adapted [31]. The SP is then given by

$$SP = (I_+ - I_-)/(I_+ + I_-)/S_{eff}, \quad (1)$$

and the spin-resolved spectra for the majority (I_{maj}) and minority spin states (I_{min}) are obtained by

$$I_{maj} = (I_+ + I_-)(1 + SP)/2, \quad (2)$$

$$I_{min} = (I_+ + I_-)(1 - SP)/2. \quad (3)$$

The angle between the magnetization direction (and also the sample surface) and x-ray was set to ∼3°. The details of the experimental geometry were described in the recently reported spin-resolved HAXPES method [31]. The excitation

photon energy was set to 5.95 keV, and total energy resolution was set to ∼0.65 eV. The binding energy (E_B) was calibrated by the Fermi level (E_F) of a Au thin film. The sample temperature was controlled by an open-cycle liquid He cryostat.

III. THEORETICAL CALCULATIONS

To obtain the partial densities of states (PDOSs) for each element of $L2_1$ stoichiometric Co_2MnSi for the simulations of HAXPES and *SP* spectra, we used the same data with the Ref. [34]. In Ref. [34], the spin-polarized electronic structures calculations at zero temperature were performed by the multiple-scattering Green's function formalism in the Korringa-Kohn-Rostoker method [35,36] implemented by HUTSEPOT code [37]. The local spin density approximation (LSDA) was used for the exchange and correlation potential [38]. The electronic structures at finite T were obtained by the disordered local moment (DLM) method [39], which corresponds to the mean-field theory of the classical statistical physics for local moments treated by the coherent potential approximation; the spin fluctuations within the mean-field approximation are treated in the calculations. Other technical details on the LSDA-DLM calculations on Co_2MnSi at finite T were described in Ref. [34].

IV. RESULTS

A. Spin-resolved valence band HAXPES of Co_2MnSi

Figure 1(a) shows the spin-integrated valence band HAXPES spectra of the MgO(2 nm)/Co_2MnSi(30 nm)/MgO (001) structure with the excitation energy of 5.95 keV measured at $T = 21$ K. The observed spectral shape is broader than those of the previously reported HAXPES spectra for bulk and thin film of Co_2MnSi [40,41], since the experimental resolution ($\Delta E \sim 0.15$eV) in the previous work is better than our ΔE of ∼0.65 eV. But the main peak, shoulder, and two humps at E_B of around 1.5, 4.0, 6.5, and 10 eV, respectively, seen in the valence band spectra [41] are commonly detected in our experiment. Figure 1(b) shows the spin-resolved valence band HAXPES spectra, which correspond to the majority and minority spin HAXPES spectra, of the Co_2MnSi thin film at $T = 21$ K. Here, the sum of the spin-resolved spectra is the same as the spin-integrated spectrum shown in Fig. 1(a). The raw data set of spin-resolved HAXPES spectra measured at $T = 21$ K is shown in Fig. S1 (see Supplemental Material [42]). The spin-resolved spectra clearly exhibit the difference in the majority and minority spin states. The majority spin spectrum shows a the metallic Fermi edge, while the minority spin spectrum shows a band gap across E_F. In Fig. 1(c), the *SP* spectrum measured at $T = 21$ K is shown. The high *SP* of ∼0.9 (∼90%) is detected at around E_F, and the *SP* spectrum shows one dip and two humps at E_B of ∼1.5, ∼3.2, and ∼7.5 eV, respectively. The high *SP* at E_F and the steep decrease of *SP* below E_F are expected to be a half-metallic nature of Co_2MnSi in the bulk region at $T = 21$ K, since HAXPES is a bulk-sensitive probe of the electronic states of solids. In our experiments, IMFP of photoelectrons emitted from the valence band is estimated to be ∼7 nm in Co_2MnSi

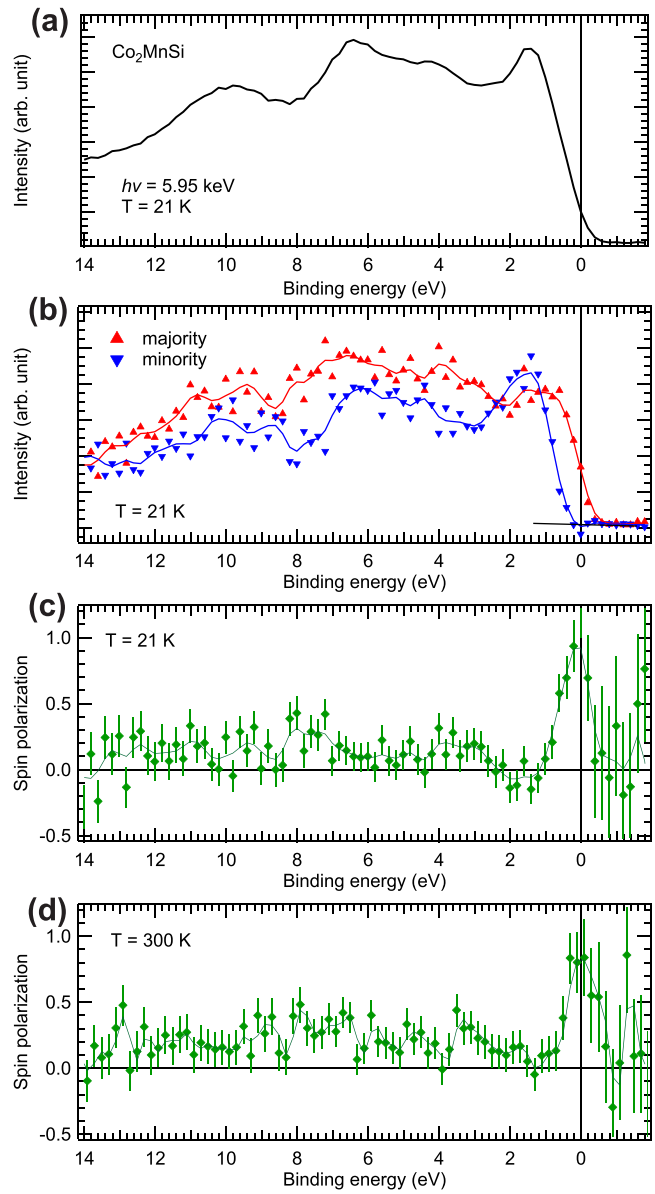

FIG. 1. Valence band HAXPES spectra of Co_2MnSi thin film. (a) Spin-integrated HAXPES spectrum obtained at $T = 21$ K. (b) Spin-resolved HAXPES spectra measured at $T = 21$ K. Thin solid lines are to guide the eye. *SP* spectra obtained at (c) $T = 21$ K and (d) 300 K. The errors of the *SP* are indicated by the vertical bars.

according to the TPP-2M (Tanuma, Powell, Penn) equation [43]. Therefore, the observed *SP* spectrum reflects not surface region but bulk one of the Co_2MnSi thin film. We have also performed the spin-resolved HAXPES measurement of the Co_2MnSi thin film at $T = 300$ K to clarify either presence or absence of T-dependent *SP*, in particular, around E_F. The *SP* spectrum measured at $T = 300$ K is shown in Fig. 1(d). Although the statistical error is large in both the *SP* spectra measured at $T = 21$ and 300 K, these spectra are similar to each other involving the high *SP* at around E_F. Therefore, Co_2MnSi in the bulk region is expected to be half-metallic even at 300 K, and shows no remarkable T dependence in the *SP* spectra. But one can see that the peak width in *SP* at

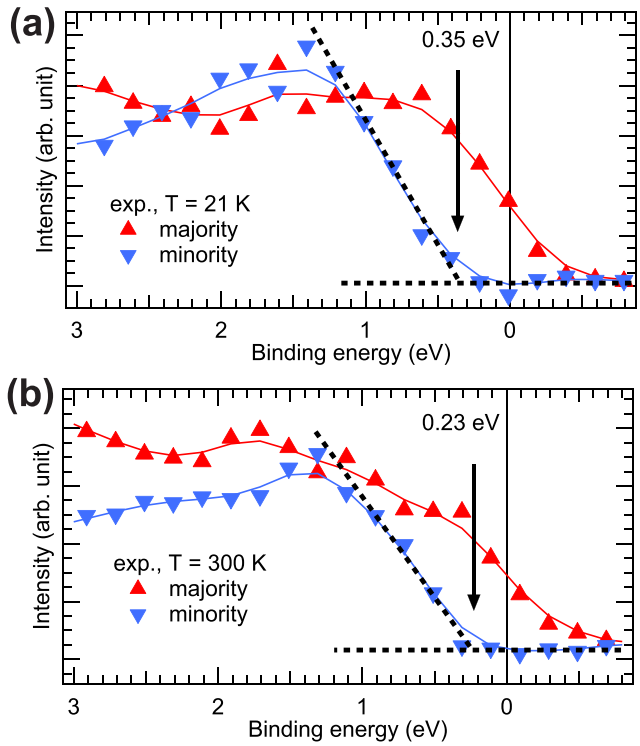

FIG. 2. Spin-resolved HAXPES spectra near E_F. (a) $T = 21$ K and (b) 300 K. Black dashed lines are to guide the eye for the minority spin VBM.

around E_F at $T = 300$ K is narrower than that at $T = 21$ K. Note that slightly positive *SP* in the wide E_B range between ~2 and 14 eV in Figs. 1(c) and 1(d) is due to the *SP* of secondary electrons, which form the background of the valence band spectra.

B. Temperature-dependent electronic states of Co_2MnSi

To look into the electronic states of Co_2MnSi in detail, the spin-resolved HAXPES spectra near E_F measured at $T =$ 21 and 300 K are shown in Fig. 2. At first glance, the minority spin spectra at both $T = 21$ and 300 K clearly show the band gap edge, which corresponds to the valence band maximum (VBM) of the minority spin states. The majority spin spectra show the metallic behavior, i.e., the finite spectral intensity goes across E_F at each T. There are no obvious intensities at E_F in the minority spin spectra at both $T = 21$ and 300 K. This result strongly suggests that the conduction band minimum (CBM) of the minority spin states is located above E_F and Co_2MnSi in the bulk region keeps a half-metallicity in the T range up to 300 K. The minority spin VBM positions at $T = 21$ and 300 K are determined by a linear extrapolation of the leading edge of the minority spin spectra, as shown in Fig. 2. The determined minority spin VBM at $T = 21$ (300) K is 0.35 (0.23) eV. The difference in VBM at $T = 21$ and 300 K is only ~0.1 eV, which would correlate with the T-dependent peak width in *SP* at around E_F as seen in Figs. 1(c) and 1(d), but spin-resolved HAXPES can clarify that the minority spin VBM of Co_2MnSi shifts as T increases. This VBM shift has not been detected by the T-dependent spin-integrated HAXPES measurements with ΔE of 0.15 eV for polycrystalline bulk Co_2MnSi [40]. Although ΔE of spin-resolved HAXPES (~0.65 eV) is larger than that of standard HAXPES (< 0.3 eV) and statistical error is large in the *SP* spectra in our experiments, the observation of the bulk-sensitive spin-resolved spectra directly reveals the shift of the minority spin VBM of the Co_2MnSi thin film as T increases. One sees that the majority spin spectra at $T = 21$ and 300 K show the different spectral shapes. This difference might be due to the photoemission Debye-Waller (DW) factor, which is a fraction of the momentum-conserved (direct) transitions [28]. In the HAXPES measurements with the photon energy of 6 keV, the DW factor is generally too low to measure the momentum-dependent electronic states by means of angle-resolved HAXPES at 300 K [28]. Therefore, the spin-resolved spectra at $T = 300$ K are governed by nondirect transitions for the Brillouin zone (BZ) averaging. The DW factor generally increases at low temperature, so that the slight increase of direct transitions might contribute to the majority and minority spin spectra, while the nondirect transitions (BZ averaging) are expected to be still dominant for the spectra at $T = 21$ K. Another possibility of the difference between the majority spin spectral shapes at $T = 21$ and 300 K might be caused by the matrix element effect [44], since we used not a polycrystalline Co_2MnSi sample but an epitaxial Co_2MnSi film sample in our experiments.

C. Simulations of HAXPES and *SP* spectra of Co_2MnSi

To visualize the PDOS contributions to the HAXPES spectra, Fig. 3 shows the cross-section weighted PDOSs (CSW-PDOSs) for each element at $T = 0$ and 300 K, where PDOSs are obtained by the LSDA-DLM calculations [34]. The per-electron cross-section ratio of Co 3*d* : Co 4*s* : Co 4*p* : Mn 3*d* : Mn 4*s* : Mn 4*p* : Si 3*s* : Si 3*p* was set to 1.00 : 20.17 : 0.757 : 0.489 : 16.74 : 0.489 : 8.258 : 0.371 according to the theoretical calculation of photoionization cross sections [45–47], where the values for the Co 4*s* and Mn 4*s* orbitals were multiplied by a factor of 2.2 to better reproduce the experimental spin-resolved HAXPES spectra. This factor might be caused by the underestimation of 4*s* PDOS in 3*d* transition metals in the PDOS calculation [48]. The total DOS and PDOSs at $T = 0$ and 300 K are shown in Figs. S2 and S3 (see Ref. [42]), respectively, for comparison. Firstly, we compare the experimental spin-resolved HAXPES spectra measured at $T = 21$ K shown in Fig. 1(b) with the CSW-PDOSs at $T = 0$ K shown in Fig. 3. One sees that the minority spin VBM and peak located at E_B of ~1.5 eV in the minority spin HAXPES spectrum in Fig. 1(b) is dominated by the Co t_{2g} minority spin states as seen in Fig. 3(a). For the majority spin HAXPES spectrum in Fig. 1(b), the structure near E_F mainly is formed by the Co e_g, t_{2g} and 4*s* majority spin states as seen in Fig. 3(a). The contribution of the Co 3*d* ($e_g + t_{2g}$) majority spin CSW-PDOS around E_F to the majority spin HAXPES spectrum is comparable to that of the Co 4*s* majority spin CSW-PDOS as seen in Fig. 3(a). Although the Co 4*s* PDOSs contribution to the total DOS is very small (see Fig. S2 in Ref. [42]), the large cross section of the Co 4*s* orbital compared to the Co 3*d* one strongly emphasizes

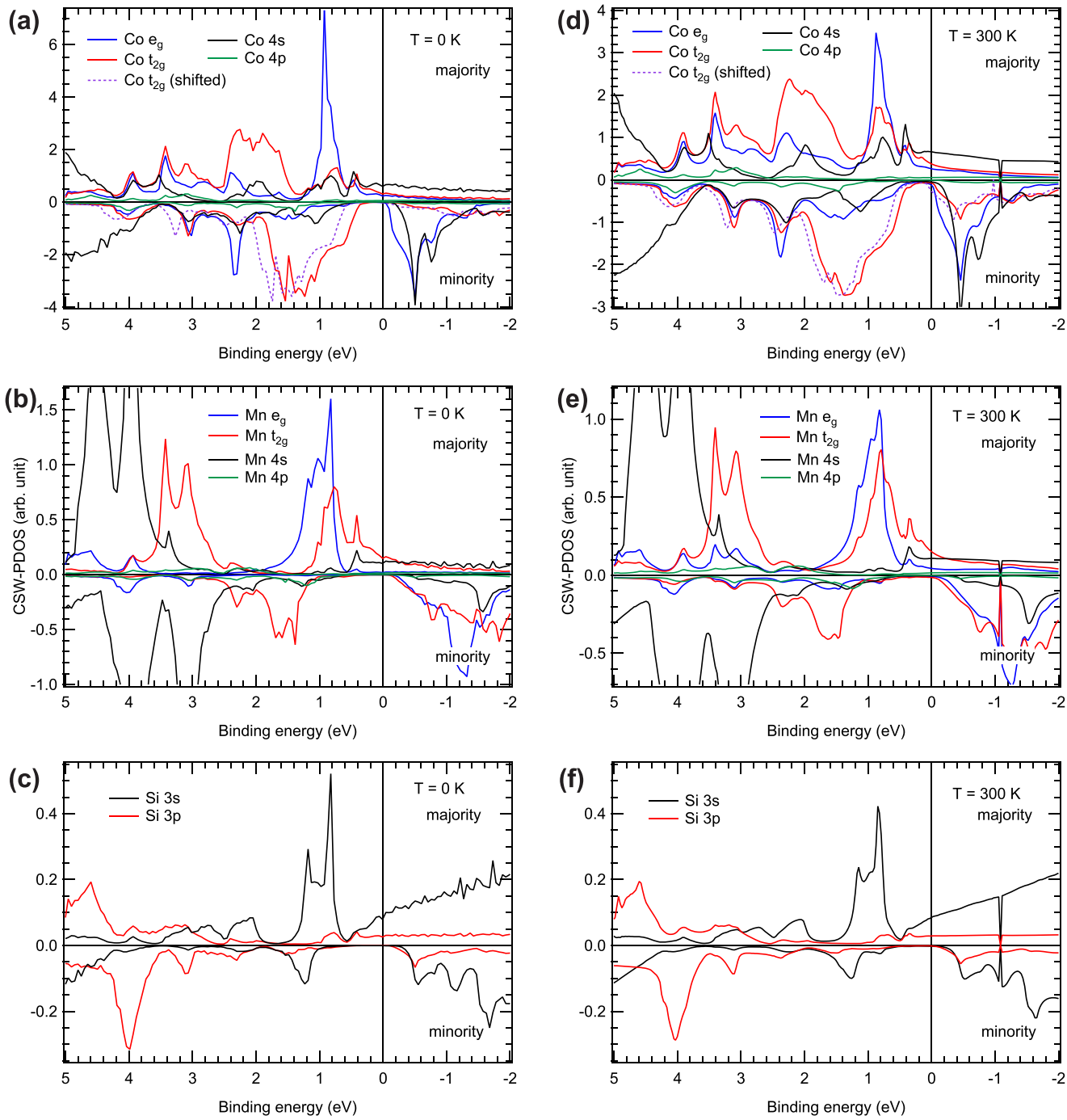

FIG. 3. Calculated spin-resolved CSW-PDOSs of Co_2MnSi. (a)–(c) CSW-PDOSs of Co, Mn, Si at $T = 0$ K. (d)-(f) CSW-PDOSs of Co, Mn, Si at $T = 300$ K. The minority spin CSW-PDOSs are shown by the negative value for visibility. The dashed lines in (a) and (d) show the shifted Co t_{2g} minority spin CSW-PDOS at each T.

the Co 4*s* states in the HAXPES spectra as reported in the 3*d* transition metals [48]. The cross section of the Mn 3*d* orbital is almost half of the Co 3*d* one, and the composition ratio of Mn to Co is 1/2 in Co_2MnSi. Therefore, the Mn 3*d* CSW-PDOS contribution to the HAXPES spectra is weak [compare Figs. 3(a) and 3(b)]. The shoulder structure at $E_B = \sim 7.0 (\sim 6.5)$ eV in the majority (minority) spin spectrum is due to the strongly emphasized Co 4*s* states, and the hump structures in the spectra at $E_B = \sim 10$ eV are mainly due to the Co 4*s* and Si 3*s* states (see Fig. S4 in Ref. [42]).

Secondly, we compare the CSW-PDOSs of Co_2MnSi at $T = 0$ K with those at $T = 300$ K in Fig. 3. Here, the energy range of the calculations at $T = 300$ K is regulated to reduce the computational resource (see Figs. S2 and S3 in Ref. [42]). At the Mn and Si sites, the CSW-PDOSs are almost unchanged with T, while those at $T = 300$ K are smoother

than at $T = 0$ K as seen in Fig. 3. In contrast, the ratios of the Co e_g CSW-PDOS to the Co t_{2g} one in both the majority and minority spin states are changed with T, although the Co 4s and 4p CSW-PDOS profiles are hardly changed with T, except for the smoothness of the profiles. In the minority spin states near E_F, one sees in Figs. 3(a) and 3(d) that the minority spin gap arising from the Co 3d states is narrower at 300 K than that at 0 K, and tail states adjacent to the minority spin VBM and CBM increase with T. The increase of the tail states leads to the slight reduction of the SP at E_F as described in Ref. [34].

Then, we have performed the simulations of the spin-resolved HAXPES and SP spectra of Co_2MnSi at $T = 0$ and 300 K for comparison with the experimental spin-resolved HAXPES and SP spectra at $T = 21$ and 300 K. In the simulation, the sum of the PDOSs multiplied by the photoionization cross sections, which is the cross-section weighted DOS (CSW-DOS), was calculated for the majority and minority spin states, for simplicity. The spin-resolved CSW-DOSs at $T = 0$ and 300 K were broadened by a Lorentzian function [full width at half maximum (FWHM) varying $\sim 0.24 \times E_B$(eV)] [48–50], then were multiplied by the Fermi-Dirac function at $T = 21$ and 300 K, respectively, and were finally broadened by a Gaussian function with FWHM of 0.64 eV. In the simulated minority spin HAXPES spectra with taking into account the shifted Co t_{2g} minority spin states, the Co t_{2g} minority spin CSW-PDOS is broadened, then is shifted to align the VBM of the minority spin spectrum in the simulations with that in the experiments at each T. The SP spectra at $T = 0$ and 300 K were calculated from the spin-resolved CSW-DOSs for each T.

Figure 4 shows the simulated HAXPES spectra at $T = 0$ and 300 K. The spectral features of the spin-resolved CSW-DOSs at $T = 0$ K shown in Fig. 4(a) roughly reproduce the experimental spectra at $T = 21$ K shown in Fig. 1(b). The simulated SP spectrum [red dotted curve in Fig. 4(b)] agrees with the experimental SP one in the higher E_B region ($E_B > 1$ eV), while the deviation between the experimental and simulated SP is clearly seen in the E_B range between 0 and 1 eV. The possible origin of the deviation between the experiment and simulation is discussed later. Since the experimental minority spin VBM at $T = 21$ K is located at $E_B = 0.35$ eV as seen in Fig. 2(a), we have adjusted the minority spin VBM in the CSW-DOS for the minority spin states on an *ad hoc* basis by the shift of the Co t_{2g} minority spin PDOS, which is indicated by black dotted curve in Fig. 4(a), where the energy shift is +0.2 eV. The corresponding SP spectrum is shown by black solid curve in Fig. 4(b). While the shift of Co t_{2g} minority spin PDOS slightly affects the CSW-DOS for the minority spin states, the SP spectrum with taking the shift into account better reproduces the experimental SP spectrum than that without taking the shift into account. The simulated HAXPES spectra at $T = 300$ K shown in Fig. 4(c) are similar to those at $T = 0$ K shown in Fig. 4(a). The simulated SP spectrum at 300 K (red dotted curve) is shown in Fig. 4(d) for comparison with the experimental SP spectrum. The minority spin VBM at $T = 300$ K in the experiment is located at $E_B = 0.23$ eV as seen in Fig. 2(b), so that we also adjusted the minority spin VBM in the simulation by the shift of the Co t_{2g} minority spin PDOS, which is indicated by black dotted

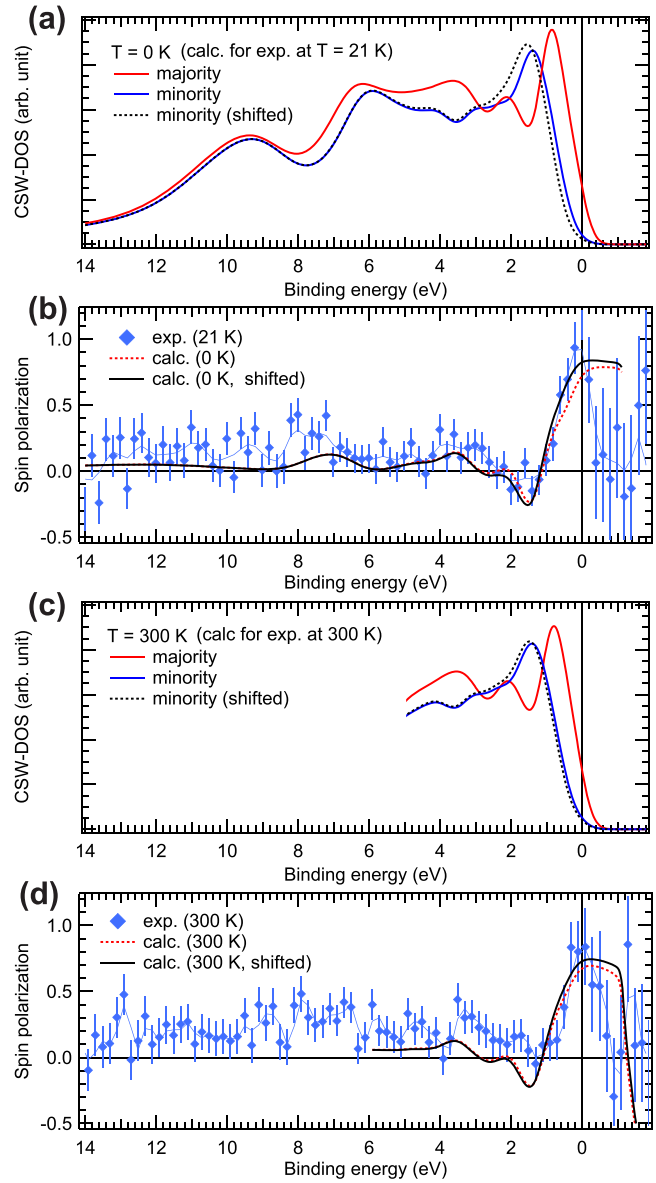

FIG. 4. Simulated spin-resolved HAXPES and SP spectra. (a) Spin-resolved CSW-DOSs of Co_2MnSi at $T = 0$ K. (b) Calculated SP spectra obtained from the CSW-DOSs at $T = 0$ K together with experimental SP spectrum at $T = 21$ K. (c) Same as (a) but $T = 300$ K. (d) Same as (b) but $T = 300$ K. The spectra shown by black dotted and solid lines in (a), (c) and (b), (d), respectively, are obtained by using the shifted Co t_{2g} minority spin PDOS. The errors of the experimental SP are indicated by the vertical bars.

curve in Fig. 4(c), where the energy shift is +0.1 eV. The corresponding SP spectrum is shown by black solid curve in Fig. 4(d). The simulated SP at E_F is increased by taking into account the shift of the minority spin VBM, and the deviation between the experiment and simulation is improved. Figure 5 shows the enlarged view of the experimental and simulated SP spectra near E_F. The improvement of deviation between the experimental and simulated SP spectra in the vicinity of E_F at $T = 21$ and 0 K, respectively, by adjusting the minority spin VBM is clearly seen, as well as that of deviation between the experimental and simulated SP at $T = 300$ K.

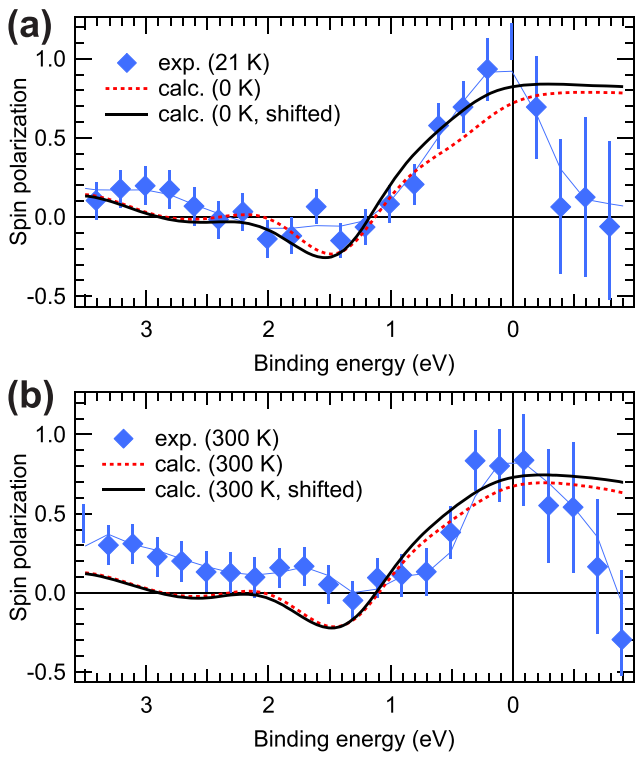

FIG. 5. Comparison between experimental and simulated *SP* spectra at around E_F. (a) Experimental *SP* spectrum at $T = 21$ K and simulated *SP* spectra at $T = 0$ K. (b) Same as (A) but $T = 300$ K for both experiment and simulation. The simulated *SP* spectra indicated by black lines in (a), (b) are obtained by using the shifted Co t_{2g} minority spin PDOS. The errors of the experimental *SP* are indicated by the vertical bars.

V. DISCUSSION

Let us consider the T-dependent spin-resolved HAXPES spectra of the epitaxial $Co_2MnSi(001)$ film shown in Fig. 2. Although the spin-integrated HAXPES of bulk polycrystalline Co_2MnSi did not show the T dependence on the valence band spectral shape [40] even in high-resolution measurements ($\Delta E \sim 0.15$ eV), our results showed the T-dependent spectral shape in the majority and minority spin spectra with $\Delta E \sim 0.65$ eV. Absence of the T-dependent spectral shape in the valence band HAXPES spectra seems to agree with the results of the T-dependent LSDA+DLM calculations [34], since the Co and Mn local site spin-resolved DOSs are almost unchanged with T in the calculations. One sees in Fig 3 (and also Figs. S2 and S3 in Ref. [42]) that the fraction of the Co e_g and t_{2g} PDOSs changes with T, although the Co local site DOSs are almost unchanged with T [34]. In contrast, the changes in the fraction of the Mn e_g and t_{2g} PDOSs are small as T is changed. It is known that the matrix element effect determines the photoelectron angular distribution, which depends on the azimuthal and magnetic quantum numbers of the occupied electrons, when the PES experiments are performed for single crystals with a linear polarized light [44]. In our experimental geometry, the photoelectron intensity detected in the electron analyzer is larger in the Co e_g states than the Co t_{2g} states due to the matrix element effect. The changes in the fraction of the Co e_g and t_{2g} states can modify the spectral shapes in the experiments. Therefore, the T-dependent majority spin spectral shape shown in Fig. 2 would be caused by the changes in the fraction of the Co e_g and t_{2g} states near E_F through the matrix element effect, while the shift and decrease of the minority spin spectral intensity with T would be due to the T dependence of the minority spin gap and the matrix element effect, respectively. In the case of polycrystalline samples, the matrix element effect is averaged by the random orientation of the crystal plane, so that the previous T-dependent HAXPES measurement on polycrystalline Co_2MnSi [40] is insensitive to the changes in the fraction of the Co e_g and t_{2g} states and is difficult to detect the shift of the minority spin VBM (~0.1 eV) without spin resolution even in high-resolution experiments. In fact, the simulated spin-integrated HAXPES spectra are almost independent on T (see Fig. S5 in Ref. [42]), while the experimental spectra (Fig. S6 in Ref. [42]) showed the T dependence mainly due to the matrix element effect.

Next, we discuss the T-dependent *SP* of Co_2MnSi. In the reported theoretical T-dependent DOS calculations for Co_2MnSi by means of LSDA+DLM [34], LSDA combined with the dynamical mean field theory [51], and the generalized gradient approximation (GGA) combined with DLM [52], it is commonly seen that the minority spin CBM is located near E_F and the tail states adjacent to the CBM cross E_F at finite T. Therefore, the calculations indicate that Co_2MnSi is no longer half-metal at finite T, while Co_2MnSi shows the half-metallicity at $T = 0$ K. Note that the *SP* at E_F calculated from total DOS at $T = 0$ K in the LSDA+DLM calculations is ~0.92 [34], which is slightly lower than 1.00 expected from the half-metallicity. This discrepancy is mainly caused by the obtained DOS from the Green's function calculated at energies including a small and finite imaginary part. And the *SP* at E_F is almost 1.0 when the smaller imaginary part is employed as described in Ref. [34]. Since the simulated *SP* spectra are based on the results of PDOS calculations in Ref. [34], the simulated *SP* at E_F shown in Figs. 4(a) and 4(b) would be slightly smaller than the case that the *SP* at E_F is 1.00 in total DOS at $T = 0$ K.

As mentioned above, to better reproduce the experimental *SP* spectra at $T = 21$ and 300 K, we adjusted the minority spin VBM by the shift of the Co t_{2g} minority spin PDOS in the simulations. This shift increased the *SP* at E_F in the simulated *SP* spectra at both $T = 0$ and 300 K as shown in Figs. 4 and 5. Since the experimental minority spin HAXPES spectra shown in Fig. 2 do not show the tail states adjacent to the minority spin CBM, which are predicted by the theoretical calculations [34,51,52], we can conclude that the minority spin CBM is expected to be located sufficiently above E_F and Co_2MnSi in the bulk region sustains high *SP* at E_F with the half-metallicity at least up to 300 K. Nawa *et al.*, showed the T dependent *SP* at E_F in total DOS of Co_2MnSi obtained by the LSDA+DLM calculations as a function of the chemical potential shift within a rigid band model [34]. The chemical potential shift reduces the decrease of the theoretical *SP* with T, when the chemical potential moves to the higher E_B side. This result also supports that the minority spin CBM is located sufficiently above E_F suggested by our experimental spin-resolved HAXPES and *SP* spectra. Note that the theoretical

minority spin gap size depends on the numerical calculation methods. For example, the GGA and LSDA calculations (T = 0 K) for Co_2MnX (X = Si, Ge, Sn) give the different minority spin gap size and the minority spin CBM position relative to E_F, while the minority spin VBM position is comparable in the calculations [8]. Since the minority spin VBM can be detectable in the spin-resolved HAXPES measurements, the direct observation method of either the minority spin gap size or minority spin CBM position is required to clarify the behaviors of T-dependent spin-resolved electronic structures of half metals.

In the above discussion, we ignored the effects of the highly spin polarized surface resonance reported in spin-resolved VUV-PES measured for the bare Co_2MnSi thin film [21] and spin-integrated soft-x-ray ARPES for AlO_x-capped Co_2MnSi thin film [25]. As mentioned in Ref. [25], the surface resonance, which comes from the six atomic layers close to the interface of AlO_x/Co_2MnSi, is dominated in soft-x-ray ARPES data due to the short IMFP of photoelectrons. In the case of HAXPES with $h\nu = 6$ keV, the intensity contribution of the surface resonance (six atomic layers) to the whole intensity is 8%, if any, when we assume that the photoelectron intensity distribution as a function of depth (d) is given by exp(-d/IMFP), where the IMFP of 7 nm is adapted. The 8% contribution of the surface resonance seems to be not so small, but the observed SP curves shown in Fig. 5 are reproduced by the simulations based on the PDOSs for bulk Co_2MnSi. This would be caused by the difference of the sample structures; the MgO-capped Co_2MnSi thin film was used for spin-resolved HAXPES in this work, whereas the bare and AlO_x-capped Co_2MnSi thin films were used in spin-resolved VUV-PES [21] and soft x-ray ARPES [25], respectively. In contrast to the positive SP in the surface resonance reported in Refs. [21,25], the first-principles calculation for the $Co_2MnSi/MgO/Co_2MnSi$ structure suggest that the SP near the interface at E_F gives a negative value due to the interface states [53]. To clarify the near interface spin-resolved electronic states (presence or absence of the interface-derived states), interface-sensitive spin-resolved HAXPES for AlO_x- and MgO-capped Co_2MnSi thin films as well as bulk-sensitive spin-resolved HAXPES for AlO_x-capped Co_2MnSi thin films is required. To perform interface-sensitive HAXPES, the tuning of the effective IMFP by using x-ray total reflection is useful as mentioned in Ref. [54], and one does not need to take into account the changes in the cross-section ratio of the atomic orbitals for the constituent elements, allowing the direct comparison of the bulk- and interface-sensitive spin-resolved electronic states of the materials capped by thin AlO_x and MgO films without considering the changes in the cross-section ratio for different excitation photon energies.

VI. SUMMARY

The T-dependent spin-resolved HAXPES measurements were conducted to directly clarify the spin-dependent valence band electronic states and SP of the 30-nm-thick epitaxial $Co_2MnSi(001)$ thin film buried under the 2-nm-thick MgO layer. At T = 21 and 300 K, the majority spin states showed the metallic Fermi edge, while the minority spin states showed a band gap across E_F, leading that the high SP at around E_F was confirmed in the bulk region of the Co_2MnSi thin film. This result suggests that Co_2MnSi in the bulk region maintains the half-metallicity up to 300 K. Although spin-resolved HAXPES was done with the low-energy resolution and the large statistical error in SP in this work, the spin-resolved HAXPES spectra directly revealed the shift of the minority spin VBM with T. The spin-resolved HAXPES spectra also revealed the slight changes in the majority spin spectral shapes with T.

We compared the experimental spin-resolved HAXPES spectra measured at T = 21 and 300 K with the simulated spectra using the PDOSs obtained by the LSDA+DLM calculations at T = 0 and 300 K. The observed T dependence of the majority and minority spin spectra was mainly caused by the changes in the Co 3d electronic states. The changes in the fraction of the Co e_g and t_{2g} PDOSs found in the T-dependent calculations would explain the slight changes in the experimental majority spin spectra with T through the matrix element effect in photoemission, since we used the epitaxial Co_2MnSi in the HAXPES experiments. The shift of the minority spin VBM mainly arose from the Co t_{2g} minority spin states. The tail states, which crossed E_F, adjacent to the minority spin CBM predicted in the calculations was not found in the experimental minority spin spectra. These results suggest that the minority spin CBM of Co_2MnSi in the bulk region is located sufficiently above E_F to keep the half-metallicity up to 300 K.

ACKNOWLEDGMENTS

The HAXPES measurements were performed with the approval of NIMS Synchrotron X-ray Station (Proposal Nos. 2020A4606 and 2020A4702). S.U. would like to thank the staff of HiSOR, Hiroshima University and JAEA at SPring-8 for the development of HAXPES at BL15XU of SPring-8. This work was partly supported by Tokodai Institute for Elemental Strategy (TIES) from The Ministry of Education, Culture, Sports, Science and Technology (MEXT), Japan [Grant No. JPMXP0112101001] and JSPS KAKENHI through a Grant-in-Aid for Scientific Research (C) [Grant No. 20K05336], (B) [Grant No. 20H02190], and (S) [Grant No. 17H06152].

[1] K. Elphick, W. Frost, M. Samiepour, T. Kubota, K. Takanashi, H. Sukegawa, S. Mitani, and A. Hirosawa, Heusler alloys for spintronic devices: Review on recent development and future perspectives, Sci. Technol. Adv. Mater. **22**, 235 (2021).

[2] Y. Nishino, H. Kato, M. Kato, and U. Mizutani, Effect of off-stoichiometry on the transport properties of the Heusler-type Fe_2Val compound, Phys. Rev. B **63**, 233303 (2001).

[3] A. Planes, L. Mansosa, and M. Accet, Magnetocaloric effect and its relation to shape-memory properties in ferromagnetic Heusler alloys, J. Phys. Condens. Matter. **21**, 233201 (2009).

[4] T. Kojima, S. Kameoka, S. Fujii, S. Ueda, and A.-P. Tsai, Catalysis-tunable Heusler alloys in selective hydrogenation of

alkynes: A new potential for old materials, Sci. Adv. **4**, eaat6063 (2018).

[5] J. Kubler, A. R. Williams, and C. B. Sommers, Formation and coupling of magnetic moments in Heusler alloys, Phys. Rev. B **28**, 1745 (1983).

[6] S. Ishida, S. Fujii, S. Kashiwagi, and S. Asano, Search for half-metallic compounds in Co_2MnZ (Z = IIIb, IVb, Vb element), J. Phys. Soc. Jpn. **64**, 2152 (1995).

[7] I. Galanakis, P. H. Dederrichs, and N. Papanikolaou, Slater-Pauling behavior and origin of the half-metallicity of the full-Heusler alloys, Phys. Rev. B **66**, 174429 (2002).

[8] S. Picozzi, A. Continenza, and A. J. Freeman, Co_2MnX (X = Si, Ge, Sn) Heusler compounds: An *ab initio* study of their structural, electronic, and magnetic properties at zero and elevated pressure, Phys. Rev. B **66**, 094421 (2002).

[9] B. Balke, G. H. Fecher, H. C. Kandpal, C. Felser, K. Kobayashi, E. Ikenaga, J.-J. Kim, and S. Ueda, Properties of the quaternary half-metal-type Heusler alloy $Co_2Mn_{1-x}Fe_xSi$, Phys. Rev. B **74**, 104405 (2006).

[10] Y. Sakuraba, M. Hattori, M. Oogane, Y. Ando, H. Kato, A. Sakuma, T. Miyazaki, and H. Kubota, Giant tunneling magnetoresistance in $Co_2MnSi/Al-O/Co_2MnSi$ magnetic tunnel junctions, Appl. Phys. Lett. **88**, 192508 (2006).

[11] T. Ishikawa, S. Hakamata, K. Matsuda, T. Uemura, and M. Yamamoto, Fabrication of fully epitaxial $Co_2MnSi/MgO/Co_2MnSi$ magnetic tunnel junctions, J. Appl. Phys. **103**, 07A919 (2007).

[12] T. Iwase, Y. Sakuraba, S. Bosu, K. Saito, S. Mitani, and K. Takanashi, Large interface spin-asymmetry and magnetoresistance in fully epitaxial $Co_2MnSi/Ag/Co_2MnSi$ current-perpendicular-to-plane magnetoresistive devices, Appl. Phys. Express **2**, 063003 (2009).

[13] T. M. Nakatani, T. Furubayashi, S. Kasai, H. Sukegawa, Y. K. Takahashi, S. Mitani, and H. Hono, Bulk and interfacial scattering in current-perpendicular-to-plane giant magnetoresistance with $Co_2Fe(Al_{0.5}Si_{0.5})$ Heusler alloy layers and Ag spacer, Appl. Phys. Lett. **96**, 212501 (2010).

[14] R. J. Soulen Jr., J. M. Byers, M. S. Osofsky, B. Nadgorny, T. Ambrose, S. F. Cheng, P. R. Broussard, C. T. Tanaka, J. Nowak, J. S. Moodera, A. Barry, and J. M. D. Coey, Measuring the spin polarization of a metal with a superconducting point contact, Science **282**, 85 (1998).

[15] Y. Bugoslavsky, Y. Miyoshi, S. K. Clowes, W. R. Branford, M. Lake, I. Brown, A. D. Caplin, and L. F. Cohen, Possibilities and limitations of point-contact spectroscopy for measurements of spin polarization, Phys. Rev. B **71**, 104523 (2005).

[16] S. Kokado, M. Tsunoda, K. Harigaya, and A. Sakuma, Anisotropic magnetoresistance effects in Fe, Co, Ni, Fe_4N, and half-metallic ferromagnet: a systematic analysis, J. Phys. Soc. Jpn. **81**, 024705 (2012).

[17] F. J. Yang, Y. Sakuraba, S. Kokado, Y. Kota, A. Sakuma, and K. Takanashi, Anisotropic magnetoresistance in $Co_2(Fe, Mn)Si$ Heusler epitaxial films: A fingerprint of half-metallicity, Phys. Rev. B **86**, 020409(R) (2012).

[18] D. Bombor, C. G. F. Blum, O. Volkonskiy, S. Rodan, S. Wurmehl, C. Hess, and B. Bucher, Half-metallic Ferromagnetism with Unexpectedly Small Spin Splitting in the Heusler Compound Co_2FeSi, Phys. Rev. Lett. **110**, 066601 (2013).

[19] K. Goto, L. S. R. Kumara, Y. Sakuraba, Y. Miura, I. Kurniawan, A. Yasui, H. Tajiri, Y. Fujita, Z. Chen, and K. Hono, Effects of the atomic order on the half-metallic electronic structure in the $Co_2Fe(Ga_{0.5}Ge_{0.5})$ Heusler alloy thin film, Phys. Rev. Mater. **4**, 114406 (2020).

[20] J.-P. Wustenberg, R. Fetzer, M. Aeschlimann, M. Cinchetti, J. Minar, J. Braun, H. Ebert, T. Ishikawa, T. Uemura, and M. Yamamoto, Surface spin polarization of the nonstoichiometric Heusler alloy Co_2MnSi, Phys. Rev. B **85**, 064407 (2012).

[21] M. Jourdan J. Minar, J. Braun, A. Kronenberg, S. Chadov, B. Balke, A. Gloskovskii, M. Kolbe, H. J. Elmers, G. Schonhense, H. Ebert, C. Felser, and M. Klaui, Direct observation of half-metallicity in the Heusler compound Co_2MnSi, Nat. Commun. **5**, 3974 (2014).

[22] S. Andriue, A. Neggache, T. Hauet, T. Devolder, A. Hallal, M. Chshiev, A. M. Bataille, P. L. Fevre, and F. Bertran, Direct evidence for minority spin gap in the Co_2MnSi Heusler compound, Phys. Rev. B **93**, 094417 (2016).

[23] S. Chernov, C. Lidig, O. Fedchenko, K. Medjanik, S. Babenknov, D. Vasilyev, M. Jourdan, G. Schonhense, and H. J. Elmer, Band structure tuning of Heusler compounds: Spin- and momentum-resolved electronic structure analysis of compounds with different band filling, Phys. Rev. B **103**, 054407 (2021).

[24] C. Guillemard, W. Zhang, G. Malinowski, C. de Melo, J. Gorchon, S. Petit-Watelot, J. Ghanbaja, S. Mangin, P. Le Fèvre, F. Bertran, and S. Andrieu, Engineering $Co_2MnAl_xSi_{1-x}$ Heusler compounds as a model system to correlate spin polarization, intrinsic gilbert damping, and ultrafast demagnetization, Adv. Mater. **32**, 1908357 (2020).

[25] C. Lidig, J. Minar, J. Braun, H. Ebert, A. Gloskovskii, J. A. Krieger, V. Strocov, M. Klau, and M. Jourdan, Surface resonance of thin film of the Heusler half-metal Co_2MnSi probed by soft x-ray angular resolved photoemission spectroscopy, Phys. Rev. B **99**, 174432 (2019).

[26] Y. Takata, M. Yabashi, K. Tamasaku, Y. Nishino, D. Miwa, T. Ishikawa, E. Ikenaga, K. Horiba, S. Shin, M. Arita, K. Shimada, H. Namatame, M. Taniguchi, H. Nohira, T. Hattori, S. Sodergren, B. Wannberg, and K. Kobayashi, Development of hard x-ray photoelectron spectroscopy at BL29XU in SPring-8, Nucl. Instrum. Methods Phys. Res. Sect. A. **547**, 50 (2005).

[27] K. Kobayashi, M. Yabashi, Y. Takata, T. Tokushima, S. Shin, K. Tamasaku, D. Miwa, T. Ishikawa, H. Nohira, T. Hattori, Y. Sugita, O. Nakatsuka, S. Sakai, and S. Zaima, High resolution-high energy x-ray photoelectron spectroscopy using third-generation synchrotron radiation source, and its application to Si-high k insulator systems, Appl. Phys. Lett. **83**, 1005 (2003).

[28] C. S. Fadley, Hard x-ray photoemission with angular resolution and standing-wave excitation, J. Electron Spectrosc. Rel. Phenom. **190**, 165 (2013).

[29] S. Ueda, Application of hard x-ray photoelectron spectroscopy to electronic structure measurements for various functional materials, J. Electron Spectrosc. Rel. Phenom. **190**, 235 (2013).

[30] X. Kozina, E. Ikenaga, C. E. V. Barbosa, S. Ouradi, J. Karel, M. Yamamoto, K. Kobayashi, H. J. Elmers, G. Schonhense, and C. Felser, Development of hard x-ray photoelectron SPLEED-based spectrometer applicable for probing of buried magnetic layer valence states, J. Electron Spectrosc. Rel. Phenom. **211**, 12 (2016).

[31] S. Ueda and Y. Sakuraba, Direct observation of spin-resolved valence band electronic states from a buried ferromagnetic layer

with hard x-ray photoemission, Sci. Technol. Adv. Mater. **22**, 317 (2021).

[32] M. Schmitt, O. Kirilmaz, S. Chernov, S. Babenkov, D. Vasilyev, O. Fedchenko, K. Medjanik, Yu. Matveyev, A. Gloskovskii, C. Schlueter, A. Winkelmann, L. Dudy, H.-J. Elmers, G. Schönhense, M. Sing, and R. Claessen, Bulk spin polarization of magnetite from spin-resolved hard x-ray photoelectron spectroscopy, Phys. Rev. B **104**, 045129 (2021).

[33] S. Ueda, Y. Katsuya, M. Tanaka, H. Yoshikawa, Y. Yamashita, S. Ishimaru, Y. Matsushita, and K. Kobayashi, Present status of the NIMS contract beamline BL15XU at SPring-8, AIP Conf Proc. **1234**, 403 (2010).

[34] K. Nawa, I. Kurniawan, K. Matsuda, Y. Miura, C. E. Patrick, and J. B. Staunton, Temperature-dependent spin polarization of Heusler Co_2MnSi from disorder local-moment approach: Effects of atomic disordering and nonstoichiometry, Phys. Rev. B **102**, 054424 (2020).

[35] J. Korringa, On the calculation of the energy of a Bloch wave in a metal, Physica **13**, 392 (1947).

[36] W. Kohn and N. Rostoker, Solution of the schrödinger equation in periodic lattices with an application to metallic lithium, Phys. Rev. **94**, 1111 (1954).

[37] M. Däne, M. Lüders, A. Ernst, D. Ködderitzsch, W. M. Temmerman, Z. Szotek, and W. Hergert, Self-interaction correction in multiple scattering theory: Application to transition metal oxides, J. Phys. Condens. Matter. **21**, 045604 (2009).

[38] J. P. Perdew and Y. Wang, Accurate and simple analytic representation of the electron-gas correlation energy, Phys. Rev. B **45**, 13244 (1992).

[39] B. L. Gyorffy, A. J. Pindor, J. Staunton, G. M. Stocks, and H. Winter, A first-principles theory of ferromagnetic phase transitions in metals, J. Phys. F Met. Phys. **15**, 1337 (1985).

[40] K. Miyamoto A. Kimura, Y. Miura, M. Shirai, M. Ye, Y. Cui, K. Shimada, H. Namatame, M. Taniguchi, Y. Takeda, Y. Saitoh, E. Ikenaga, S. Ueda, K. Kobayashi, and T. Kanomata, Absence of temperature dependence of the valence-band spectrum of Co_2MnSi, Phys. Rev. B **79**, 100405(R) (2009).

[41] G. H. Fecher, B. Balke, A. Gloskowskii, S. Ouardi, C. Felser, T. Ishikawa, M. Yamamoto, Y. Yamashita, H. Yoshikawa, S. Ueda, and K. Kobayashi, Detection of the valence band in buried Co_2MnSi-MgO tunnel junctions by means of photoemission spectroscopy, Appl. Phys. Lett. **92**, 193513 (2008).

[42] See Supplemental Material at http://link.aps.org/supplemental/10.1103/PhysRevB.106.075101 for raw data at 21 K, spin-resolved PDOSs at 0 and 300 K, spin-resolved CSW-PDOSs at 0 K, and simulated and experimental spin-integrated HAXPES spectra.

[43] S. Tanuma, C. J. Powell, and D. R. Penn, Calculations of electron inelastic mean free paths. V. Data for 14 organic coumpounds over the 50–2000 eV range, Surf. Interf. Anal. **21**, 165 (1993).

[44] S. M. Goldberg, C. S. Fadley, and S. Kono, Photoionization cross sections for atomic orbitals with random and fixed spatial orientation, J. Electron Spectrosc. Rel. Phenom. **21**, 285 (1981).

[45] J. H. Scofield, Theoretical photoionization cross sections from 1 to 1500 keV Tech. Rep. UCRL-51326, Lawrence Livermore Laboratory, 1973.

[46] M. B. Trzhaskovskaya, V. I. Nefedov, and V. G. Yarzhemsky, Photoelectron angular distribution parameters for elements z = 1 to 54 in the photoelectron energy range 100–5000eV. At. Data Nucl. Data Tables **77**, 97 (2001).

[47] M. B. Trzhaskovskaya, V. K. Nikulin, V. I. Nefedov, and V. G. Yarzhemsky, Non-dipole second order parameters of the photoelectron angular distribution for elements Z = 1-100 in the photoelectron energy range 1–10 keV. At. Data Nucl. Data Tables **92**, 245 (2006).

[48] S. Ueda and I. Hamada, Polarization dependent bulk-sensitive valence band photoemission spectroscopy and density functional calculations: Part I. 3d transition metals, J. Phys. Soc. Jpn. **86**, 124706 (2017).

[49] J. Park, K. H. Kim, H.-J. Noh, and S.-J. Oh, Photoemission and x-ray absorption spectroscopy studies on cubic pyrochlore ruthenates $Bi_{2-x}Y_xRu_2O_7$, Phys. Rev. B **69**, 165120 (2004).

[50] S. Ueda, M. Mizuguchi, Y. Miura, J. G. Kang, M. Shirai, and K. Takanashi, Electronic structure and magnetic anisotropy of $L1_0$-FePt thin film studied by hard x-ray photoemission spectroscopy and first-principles calculation, Appl. Phys. Lett. **109**, 042404 (2016).

[51] L. Chioncel, Y. Sakuraba, E. Arrigoni, M. I. Katsenelson, M. Oogane, Y. Ando, T. Miyazaki, E. Burzo, and A. I. Lichtenstein, Nonquasiparticle States in Co_2MnSi Evidenced Through Magnetic Tunnel Junction Spectroscopy Measurements, Phys. Rev. Lett. **100**, 086402 (2008).

[52] H. Shinya, S. Kou, T. Fukushima, A. Masago, K. Sato, H. Katayama-Yoshida, and H. Akai, First-principles calculations of finite temperature electronic structures and transport properties of Heusler alloy Co_2MnSi, Appl. Phys. Lett. **117**, 042402 (2020).

[53] Y. Miura, H. Uchida, Y. Oka, K. Abe, and M. Shirai, Half-metallic interface and coherent tunneling in $Co_2YZ/MgO/Co_2YZ$ (YZ = MnSi, CrAl) magnetic tunnel junctions: A first-principles study, Phys. Rev. B **78**, 064416 (2008).

[54] S. Ueda, Depth-resolved electronic structure measurements by hard x-ray photoemission combined with x-ray total reflection: Direct probing of surface band bending of polar GaN, Appl. Phys. Express **11**, 105701 (2018).